Adaptive IMM-Based Smoothing Probabilistic Data Association for Maneuvering Target Tracking in Cluttered Environments

Yi CHENG [1,2], Xinyu ZHANG [1,2], Yingying YAN [1]

[1] School of Control Science and Engineering, Tiangong University, Bin Shui West Road 399, Tianjin, 300387, China
[2] School of Control Science and Engineering, Tianjing Key Laboratory of Intelligent Control for Electrical Equipment, Tiangong University, Bin Shui West Road 399, Tianjin, 300387, China

chengyi@tiangong.edu.cn, zhxyme@163.com, 15942403547@163.com

Submitted July 23, 2025 / Accepted December 1, 2025 / Online first December 22, 2025

Abstract. *Modern radar systems face many challenges, including complex nonlinear motion modelling, real-time changes of target motion model and difficult target trajectory estimation under low signal noise ratio when tracking high maneuvering targets in a cluttered environment. Therefore, an improved probabilistic data association tracking algorithm, termed adaptive transition probability matrix and improved smoothing integrated probabilistic data association (ATPM-ISIPDA) by embedding adaptive interactive multiple models (IMM) and parallel cubature information filter (PCIF) is proposed. Based on the fixed-lag smoothing integrated probabilistic data association (FLSIPDA) and IMM framework, the proposed algorithm uses the model posterior information to adaptively adjust the model transition probability, thereby enhancing model matching accuracy. Additionally, the parallel cubature information filter (PCIF) is utilized in each IMM sub-filter to suppress the state estimation error of nonlinear systems. In the fusion stage, the multi-branch cubature Kalman filter (CKF) prediction results are fused by the weighted accumulation method of the information matrix and vector, and the optimized smoothed state predictions and covariance matrices are generated. Then, the smoothed component data association probability is calculated to obtain the final state estimate, enhancing the fusion and smoothing performance of forward and backward tracks. The simulation results show that compared to the traditional IMM-IPDA algorithm, the average position RMSE is reduced by 31.1%, the FTD accuracy is improved by 15%–20%, and it still maintains a good tracking confirmation rate in cluttered environments.*

Keywords

ATPM, data association, smoothing, false-track discrimination, parallel cubature information filter

1. Introduction

Radar systems are widely used in both military and civilian applications. However, in an unknown environment, radar measurements are contaminated by noise, clutter and interference. In this scenario, the measurements generated by clutter tend to cluster near the target's true position, interfering with the target's predicted trajectory and making it difficult to distinguish the true trajectory. Additionally, the target's maneuverability and low detection probability result in unreliable prior motion information. Consequently, tracking maneuvering targets in cluttered environments remains a significant challenge [1], [2].

1.1 Nonlinear Filtering for Maneuvering Target Tracking

The classic Kalman filter can effectively track single-model targets but exhibits performance degradation for maneuvering targets due to model mismatch, leading to filter divergence. The interacting multiple model (IMM) algorithm was developed based on the generalized pseudo-Bayesian framework [3], where multiple dynamic models are probabilistically fused to achieve effective tracking of maneuvering targets. Given that true targets often operate within nonlinear systems, the linear Kalman Filter (KF) is not well-suited for radar's nonlinear measurement systems. Therefore, nonlinear filtering algorithms, including the unscented Kalman filter (UKF), cubature Kalman filter (CKF) and particle filter (PF) had been integrated with IMM frameworks [4], [5] to enhance the processing ability of nonlinear systems.

1.2 Adaptive Transition Probability Matrix Algorithms

However, the fixed Markov transition probability matrix of IMM may still have the target's inaccurate prior information, leading to mismatches in complex scenarios. Therefore, the model likelihood functions were used in [6] to update the

DOI: 10.13164/re.2026.0026

transition probability adaptively, improving model matching probability. However, this approach tends to lead to likelihood function singularity and filter divergence. Reference [7] used variational inference to achieve joint estimation of kinematic and shape states for maneuvering extended targets, incorporating an adaptive model transition probability. However, the performance of this approach may degrade under conditions of high computational load or when tracking non-elliptical target shapes. Moreover, based on the Bayesian framework, two model IMM algorithms and model jump thresholds were utilized to update the transition probability matrix in real time [8]. However, the local errors will be increased during stable model periods and add computational complexity due to their parallel processing implementation. Furthermore, the Q-learning-based adaptive transition probability strategy, proposed in [9], was embedded into IMM to mitigate model-switching lag, but filter divergence may still be triggered by reward-function noise sensitivity and premature Q-value initialization.

1.3 Data Association and Smoothing in Cluttered Environments

In addition, in actual radar measurements, measurements are often contaminated by clutter and interference, with true target measurements often obscured by false returns. Therefore, data association algorithms are adopted to solve the observation trajectory matching problem, while false track discrimination (FTD) techniques validate the real tracks. Traditional data association algorithms, like probabilistic data association (PDA) [10] and multiple hypothesis tracking (MHT) [11], were used to solve measurement association but lack FTD capability. Later, the target existence probability was first proposed in integrated probabilistic data association (IPDA) [12], which was utilized as the primary metric for assessing track quality in FTD. Furthermore, smoothing algorithms utilize future measurements to estimate the target state in past scans, reducing estimation errors and improving tracking performance. Typical smoothing techniques include fixed-interval smoothing IPDA (sIPDA), fixed lag smoothing IPDA (FLSIPDA) and fixed-interval integrated track splitting smoothing (ITS-S) [13–15], which leverage the smoothed probability of target existence to enhance FTD. Moreover, these algorithms were extended to the multi-target tracking environment [16]. By using multiple models and target existence state information, an interacting multiple models integrated probabilistic data association (IMM-IPDA) algorithm was proposed [17]. In order to smooth probability of target existence, the augmented fixed-lag smoothing was used that considered all feasible multi-scan target existence events [18]. However, the fixed-lag window restricts maneuver adaptability. In addition, the forward-backward prediction model was used to achieve smooth state estimation [19]. However, this model faces challenges in achieving a balanced fusion of forward and backward prediction.

1.4 Information Filtering for State Estimation

Therefore, the information filtering (IF) was used to transform the state estimation into a linear superposition structure through the information form to improve the numerical stability [20]. But its inverse matrix calculation leads to a large error in multi-model state estimation. The extended information filtering (EIF) can alleviate the linearization system error [21], but it is difficult to meet the requirements of high maneuvering target tracking accuracy. Therefore, the cubature information filter (CIF) was used [22] to accurately calculate the nonlinear integral through the third-order spherical-radial cubature rules, but it is vulnerable to the influence of non-positive covariance, leading to filter divergence. A summary of the discussed methods and their main limitations is provided in Tab. 1.

Building upon analysis of existing methods, two critical limitations in current tracking algorithms are identified. 1) Model-switching lag during maneuvers is caused by fixed transition probability matrix in traditional interacting multiple model (IMM). 2) Nonlinear estimation errors and imbalanced forward-backward fusion arise from linear fusion in fixed-lag smoothing integrated probabilistic data association (FLSIPDA). To solve these, an adaptive transition probability matrix improved smoothing integrated probabilistic data association (ATPM-ISIPDA) algorithm is proposed. Its main contributions, explicitly linked to advancements in existing methods, are summarized as follows

- An adaptive transition probability matrix (ATPM) is proposed to solve the model-switching lag inherent in traditional fixed-matrix IMM. The proposed matrix is dynamically adjusted using real-time posterior information, effectively enhancing model-matching capability during maneuvering transitions.
- A parallel cubature information filter (PCIF) is proposed to resolve nonlinear estimation inaccuracy and fusion imbalance in traditional smoothing algorithms. An integration of forward and backward state estimations is achieved through parallel fusion of multi-branch CKF predictions using the spherical-radial cubature rule.
- A unified algorithmic framework is established by integrating the ATPM and PCIF into the IMM and FLSIPDA smoother. This integration allows the proposed ATPM-ISIPDA algorithm to enhance model-matching accuracy and smoothing robustness, effectively overcoming the performance trade-offs inherent in existing tracking methods.
- A comprehensive performance evaluation is conducted through extensive simulations. The results validate that the proposed algorithm achieves improvements in both tracking accuracy and false track discrimination capability compared with several traditional algorithms.

Method category	Core idea	Advantages	Limitations
Fixed-matrix IMM	Multiple models with constant transition probability	Effective for known maneuver patterns	Noise-induced initialization bias
Adaptive IMM [6–9]	Adjust transition probability adaptively	Improved model matching	Likelihood function singularity [6]; variational overload [7]; High complexity [8]; noise sensitivity [9]
Smoothing algorithms [13–19]	Use future measurements for smoothing	Improved accuracy and FTD	Limited maneuver adaptability [18]; Imbalanced forward-backward fusion [19]
Information filtering [20–22]	State estimation in information form	Improved numerical stability	Errors in the inverse matrix [20]; Difficult to meet tracking accuracy [21]; Vulnerability to non-positive covariance in CIF [22]
ATPM-ISIPDA	Integrates adaptive transition probability matrix and parallel cubature information filter with an IMM-FLSIPDA framework	Superior model-matching and smoothing performance in clutter	Moderately increased computational load due to the parallel filtering structure and smoothing logic

Tab. 1. Summary of existing tracking methods and their limitations.

The core problem of maneuvering target tracking addressed in this work represents a significant challenge in signal processing for radar, a fundamental wireless sensing technology. This paper is organized as follows. Section 2 presents the target motion and measurement models. In Sec. 3, a correction factor is defined based on model posterior probabilities to adaptively adjust the transition probability matrix, followed by a detailed analysis of its impact on IMM algorithm performance. Furthermore, the weighted accumulation fusion method in the form of information is proposed to realize the balance of forward and backward prediction. Building upon this, combined with the traditional smoothing algorithm, the ATPM-ISIPDA algorithm is proposed. In Sec. 4, the simulation tests are carried out under various scenarios to verify the performance of the ATPM-ISIPDA algorithm. Section 5 summarizes the ATPM-ISIPDA algorithm.

2. Target Motion Model

The target trajectory state at each scan is modelled by a discrete-time nonlinear hybrid dynamics system and the measurement equation.

$$\begin{aligned} \mathbf{x}_k &= \mathbf{F}\mathbf{x}_{k-1} + \mathbf{G}\mathbf{u}_{k-1} + \mathbf{B}\mathbf{v}_{k-1}, \\ \mathbf{z}_k &= \mathbf{H}\mathbf{x}_k + \mathbf{w}_k \end{aligned} \tag{1}$$

where $\mathbf{x}_{k-1}$ is the state of the system at time $k-1$, $\mathbf{z}_k$ is the measurment of radar at time k, and $\mathbf{u}_{k-1}$ is the input vector. The process noise $\mathbf{v}_{k-1}$ and measurement noise $\mathbf{w}_k$ are zero-mean white Gaussian noises with covariances $\mathbf{Q}_k$ and $\mathbf{R}_k$, respectively.

The state vector $\mathbf{x}_k$ of $n\times 1$ dimension includes the position, velocity and acceleration in the radar coordinate system.

$$\mathbf{x}_k = [x\ \dot{x}\ \ddot{x}\ y\ \dot{y}\ \ddot{y}\ z\ \dot{z}\ \ddot{z}]^{\mathrm{T}}. \tag{2}$$

The target will have three motion models to form its trajectory. The following equations are all general models in the field of radar target tracking. For the constant velocity (CV) model, the state transition matrix $\mathbf{F}_{\mathrm{CV}}$ and the process noise matrix $\mathbf{Q}_{\mathrm{CV}}$ are given in (3) and (4):

$$\mathbf{F}_{\mathrm{CV}} = \mathrm{diag}[\mathbf{f}_{\mathrm{CV}}, \mathbf{f}_{\mathrm{CV}}, \mathbf{f}_{\mathrm{CV}}], \tag{3}$$

$$\mathbf{Q}_{\mathrm{CV}} = \mathrm{diag}[\mathbf{q}_{\mathrm{CV}}, \mathbf{q}_{\mathrm{CV}}, \mathbf{q}_{\mathrm{CV}}] * q \tag{4}$$

where T is the sampling time, q denotes the plant noise parameter. This 3×3 formulation for $\mathbf{f}_{\mathrm{CV}}$, which corresponds to the three state variables (position, velocity, acceleration) in one coordinate direction, shares the same dimensionality as the $\mathbf{f}_{\mathrm{CA}}$ matrix in (9) to maintain consistency across linear motion models. The specific forms of $\mathbf{f}_{\mathrm{CV}}$ and $\mathbf{q}_{\mathrm{CV}}$ are given as

$$\mathbf{f}_{\mathrm{CV}} = \begin{bmatrix} 1 & T & 0 \\ 0 & 1 & 0 \\ 0 & 0 & 0 \end{bmatrix}, \tag{5}$$

$$\mathbf{q}_{\mathrm{CV}} = \begin{bmatrix} \frac{T^3}{3} & \frac{T^2}{2} & 0 \\ \frac{T^2}{2} & T & 0 \\ 0 & 0 & 0 \end{bmatrix}. \tag{6}$$

For the constant acceleration (CA) model, the state transition matrix $\mathbf{F}_{\mathrm{CA}}$ and the process noise matrix $\mathbf{Q}_{\mathrm{CA}}$ are given in (7) and (8):

$$\mathbf{F}_{\mathrm{CA}} = \mathrm{diag}[\mathbf{f}_{\mathrm{CA}}, \mathbf{f}_{\mathrm{CA}}, \mathbf{f}_{\mathrm{CA}}], \tag{7}$$

$$\mathbf{Q}_{\mathrm{CA}} = \mathrm{diag}[\mathbf{q}_{\mathrm{CA}}, \mathbf{q}_{\mathrm{CA}}, \mathbf{q}_{\mathrm{CA}}] * q \tag{8}$$

where parameters $\mathbf{f}_{\mathrm{CA}}$ and $\mathbf{q}_{\mathrm{CA}}$ are three-dimensional matrix given as

$$\mathbf{f}_{\mathrm{CA}} = \begin{bmatrix} 1 & T & \frac{T^2}{2} \\ 0 & 1 & T \\ 0 & 0 & 1 \end{bmatrix}, \tag{9}$$

$$\mathbf{q}_{\mathrm{CA}} = \begin{bmatrix} \frac{T^5}{20} & \frac{T^4}{8} & \frac{T^3}{6} \\ \frac{T^4}{8} & \frac{T^3}{3} & \frac{T^2}{2} \\ \frac{T^3}{6} & \frac{T^2}{2} & T \end{bmatrix}. \tag{10}$$

For the coordinate turn (CT) model, the state transition matrix $\mathbf{F}_{\mathrm{CT}}$ and the process noise matrix $\mathbf{Q}_{\mathrm{CT}}$ are given in (11) and (12):

$$\mathbf{F}_{\mathrm{CT}} = \mathrm{diag}[\mathbf{f}_{\mathrm{CT}}, \mathbf{f}_{\mathrm{CT}}, \mathbf{f}_{\mathrm{CT}}], \tag{11}$$

$$\mathbf{Q}_{\mathrm{CT}} = \mathrm{diag}[\mathbf{q}_{\mathrm{CT}}, \mathbf{q}_{\mathrm{CT}}, \mathbf{q}_{\mathrm{CT}}] * q \tag{12}$$

where ω denotes the coordinated turn rate. In contrast to the CV and CA models, the CT model incorporates the turn rate ω as a state variable to characterize angular motion. Consequently, its state-transition matrix $\mathbf{f}_{\mathrm{CT}}$ is formulated as a 4×4 matrix to account for the coupling between the turn rate and the kinematic states (position and velocity). The specific structure of $\mathbf{f}_{\mathrm{CT}}$ and its associated process noise matrix $\mathbf{q}_{\mathrm{CT}}$ are defined as follows

$$\mathbf{f}_{\mathrm{CT}} = \begin{bmatrix} 1 & \frac{\sin(\omega T)}{\omega} & 0 & \frac{(\cos(\omega T)-1)}{\omega} \\ 0 & \cos(\omega T) & 0 & -\sin(\omega T) \\ 0 & -\frac{(\cos(\omega T)-1)}{\omega} & 1 & \frac{\sin(\omega T)}{\omega} \\ 0 & \sin(\omega T) & 0 & \cos(\omega T) \end{bmatrix}, \tag{13}$$

$$\mathbf{q}_{\mathrm{CT}} = \begin{bmatrix} \frac{T^3}{3} & \frac{T^2}{2} & 0 \\ \frac{T^2}{2} & T & 0 \\ 0 & 0 & 0 \end{bmatrix}. \tag{14}$$

The nonlinear measurement of the radar include the distance R, the pitch angle α, and the azimuth angle β, and the systematic measurement equation can be established.

$$\mathbf{Z}_k = \begin{bmatrix} R & \alpha & \beta \end{bmatrix}^{\mathrm{T}} = \begin{bmatrix} \sqrt{x^2+y^2+z^2} \\ \arctan(\frac{z}{\sqrt{x^2+y^2}}) \\ \arctan(\frac{y}{x}) \end{bmatrix} + \mathbf{v}_k. \tag{15}$$

3. The Design of the ATPM-ISIPDA Algorithm

This section details the design of the ATPM-ISIPDA algorithm. Specifically, an adaptive transition probability matrix (ATPM) is proposed in Sec. 3.1 to address the limitations of fixed transition probability matrix. Subsequently, a parallel cubature information filter (PCIF) is proposed in Sec. 3.2 to mitigate errors in nonlinear filtering scenarios. Finally, Section 3.3 integrates ATPM and PCIF into IMM and the fixed-lag smoothing integrated probabilistic data association (FLSIPDA) framework, and outlines the complete workflow of the ATPM-ISIPDA algorithm.

3.1 The Improvement of the Transition Probability Matrix

The IMM algorithm assumes that the model probability is transformed through a Markov chain. The classical IMM algorithm includes five processes: 1) model interaction, 2) model estimation, 3) model likelihood function updating, 4) model probability updating, and 5) state estimation fusion [23].

However, in the model interaction stage, the fixed probability transition matrix fails to accurately capture actual model switching with target maneuvering, resulting in increased estimation errors [24]. Consequently, an improved adaptive transition probability matrix (ATPM) is proposed, which utilizes the posterior information to set adjustment coefficients for each element of the matrix, making the switching between models more reasonable. The improved algorithm process is presented below, with the corresponding flowchart depicted in Fig. 1.

Due to the non-negativity value of the model transition probability and the IMM contains N motion models, the model probability change rate is defined as

$$\boldsymbol{\psi}_{ij}(k) = \boldsymbol{\varphi}_{ij}(k) \cdot \boldsymbol{\kappa}_j(k) \tag{16}$$

where $\boldsymbol{\varphi}_{ij}(k)$ denotes the model transition correction function and $\boldsymbol{\kappa}_j(k)$ represents the model probability conversion rate.

$$\boldsymbol{\kappa}_j(k) = \exp[\boldsymbol{\mu}_j(k) - \boldsymbol{\mu}_j(k-1)],\ j = 1, \ldots N. \tag{17}$$

At time k, let $u_j(k)$ and $u_i(k)$ represent the probabilities of the models of models j and i, respectively. The gradient of the model probability $\Delta u_j(k) = u_j(k) - u_j(k-1)$ is used to represent its variation trend. When $\Delta u_j(k) > 0$, $\boldsymbol{\kappa}_j(k) > 1$, the correction trend is to increase the transition probability from other models to the model j, but it cannot be judged that the model j is the matched model at the moment. Therefore, for the model i, whose gradient $\Delta u_i(k) < 0$, and correction function $\boldsymbol{\kappa}_j(k) < 1$, which indicates that the model j is considered the matched model. On the other hand, if $\Delta u_i(k) > 0$, $\Delta u_i(k) \geq \Delta u_j(k)$, the model i is considered the matched model and the transition probability from the model i to the model j should be suppressed; else if $\Delta u_i(k) > 0$, $\Delta u_i(k) < \Delta u_j(k)$, the model i is considered the matched model and the transition probability from the model i to the model j should be increased. Similarly, when $\Delta u_j(k) < 0$, the transition probability will also be adjusted according to the same logic.

Based on the conditions, $\boldsymbol{\varphi}_{ij}(k)$ is given by

$$\boldsymbol{\varphi}_{ij}(k) = \left(\frac{\exp[\boldsymbol{\mu}_j(k) - \boldsymbol{\mu}_j(k-1)]}{\exp[\boldsymbol{\mu}_i(k) - \boldsymbol{\mu}_i(k-1)]} \right)^{\beta},\ i, j = 1, \ldots, N \tag{18}$$

where β is the correction rate and $0 < \beta < 1$.

Based on (18), the modified Markov matrix that satisfies two basic requirements [25] can be obtained as

$$\boldsymbol{\pi}'_{ij}(k) = \frac{\boldsymbol{\psi}_{ij}(k)\boldsymbol{\pi}_{ij}}{\sum_{i=1}^{N} \boldsymbol{\psi}_{ij}(k)\boldsymbol{\pi}_{ij}} = \frac{\boldsymbol{\varphi}_{ij}(k)\boldsymbol{\kappa}_j(k)\boldsymbol{\pi}_{ij}}{\sum_{i=1}^{N} \boldsymbol{\varphi}_{ij}(k)\boldsymbol{\kappa}_j(k)\boldsymbol{\pi}_{ij}}. \tag{19}$$

3.2 Parallel Cubature Information Filter

Although the ATPM module effectively stabilizes model adaptation, it does not directly mitigate clutter-induced

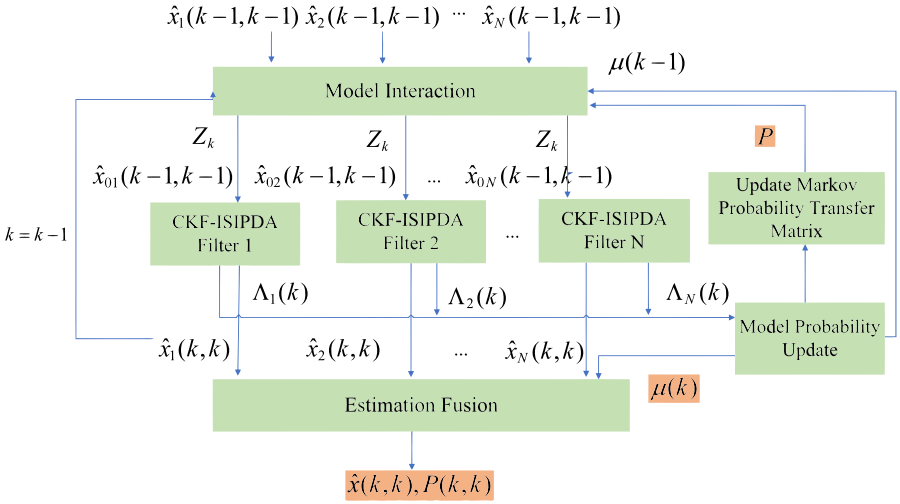

Fig. 1. Adaptive transition probability matrix algorithm.

false measurements, which is a critical challenge in dense clutter environments. To mitigate this limitation, the traditional FLSIPDA smoothing algorithm uses information filtering (IF) for both forward and backward fusion stages to enhance the reliability of measurement association. However, IF relies on linear weighting operations, which can increase forward and backward prediction state errors in highly nonlinear system dynamics or during abrupt target state maneuvers. This can result in the loss of fusion components and distortion in the calculation of smoothing association probabilities, thereby affecting the accuracy of state estimation. Therefore, a parallel cubature information filter (PCIF) is proposed, which is used in the FLSIPDA algorithm to replace the IF filter. PCIF utilizes its internal multiple parallel CKF branches to generate nonlinear state predictions during the prediction stages of the forward and backward tracks in FLSIPDA. It then converts these predictions into information matrices and vectors by operating in the information form. Subsequently, it uses the weighting mechanism to fuse the converted forward and backward state predictions to generate a set of optimized smoothed information estimates. This optimized output enhances the data association probability, thereby improving smoothing performance and state estimation accuracy. The improved algorithm process is shown in Fig. 2.

1. Given N sensors, the Cubature Kalman Filter (CKF) prediction step computes each model's target state vector $\hat{\mathbf{x}}_{k|k-1}$ and error covariance matrix $\mathbf{P}_{k|k-1}$. These are then transformed into the information matrix $\boldsymbol{\delta}_{k|k-1}$ and information vector $\boldsymbol{\gamma}_{k|k-1}$.

$$\boldsymbol{\delta}_{k|k-1} = \mathbf{P}_{k|k-1}^{-1}, \tag{20}$$

$$\boldsymbol{\gamma}_{k|k-1} = \boldsymbol{\delta}_{k|k-1}\hat{\mathbf{x}}_{k|k-1}, \tag{21}$$

$$\hat{\mathbf{x}}_{k|k-1} = \frac{1}{2n}\sum_{i=1}^{2n}\mathbf{x}^*_{i,k|k-1}, \tag{22}$$

$$\mathbf{P}_{k|k-1} = \frac{1}{2n}\sum_{j=1}^{2n}(\mathbf{x}^*_{j,k|k-1} - \hat{\mathbf{x}}_{k|k-1})(\mathbf{x}^*_{j,k|k-1} - \hat{\mathbf{x}}_{k|k-1})^{\mathrm{T}} + \mathbf{Q}_{k-1} \tag{23}$$

where $\mathbf{x}^*_{i,k|k-1}$ is the propagation cubature point of the nonlinear function.

2. According to the predicted measurement $\hat{\mathbf{z}}_{k|k-1}$ and cubature point $\mathbf{z}^*_{i,k|k-1}$, the corresponding information state contribution of each measurement is calculated.

$$\mathbf{I}_k^i = \boldsymbol{\delta}^i_{k|k-1}\mathbf{P}^i_{xz,k|k-1}(\mathbf{R}^i_k)^{-1}(\boldsymbol{\delta}^i_{k|k-1}\mathbf{P}^i_{xz,k|k-1})^{\mathrm{T}}, \tag{24}$$

$$\mathbf{i}_k^i = \boldsymbol{\delta}^i_{k|k-1}\mathbf{P}^i_{xz,k|k-1}(\mathbf{R}^i_k)^{-1}\left[\mathbf{z}^i_k - \hat{\mathbf{z}}_{k|k-1} + \mathbf{P}^i_{xz,k|k-1}\boldsymbol{\gamma}^i_{k|k-1}\right], \tag{25}$$

$$\mathbf{P}^i_{xz,k|k-1} = \frac{1}{2n}\sum_{j=1}^{2n}(\mathbf{x}^*_{j,k|k-1} - \hat{\mathbf{x}}_{k|k-1})(\mathbf{z}^*_{j,k|k-1} - \hat{\mathbf{z}}_{k|k-1})^{\mathrm{T}}. \tag{26}$$

3. Subsequently, the information matrix $\boldsymbol{\delta}_{k|k}$ and information vector $\boldsymbol{\gamma}_{k|k}$ for each measurement at time k are computed as

$$\boldsymbol{\delta}_{k|k} = \boldsymbol{\delta}_{k|k-1} + \sum_{i=1}^{N}\mathbf{I}^i_k, \tag{27}$$

$$\boldsymbol{\gamma}_{k|k} = \boldsymbol{\gamma}_{k|k-1} + \sum_{i=1}^{N}\mathbf{i}^i_k. \tag{28}$$

4. The modified information vector is subsequently transformed into its corresponding state value and covariance representation as follows.

$$\hat{\mathbf{x}}_{k|k} = \mathbf{P}_{k|k}\boldsymbol{\gamma}_{k|k}, \tag{29}$$

$$\mathbf{P}_{k|k} = \boldsymbol{\delta}^{-1}_{k|k}. \tag{30}$$

Compared to conventional EKF/UKF, PCIF with a multi-model framework unifies the time update and measurement update procedures. It effectively suppresses nonlinear approximation errors, thereby enhancing both stability and estimation consistency of the state estimation.

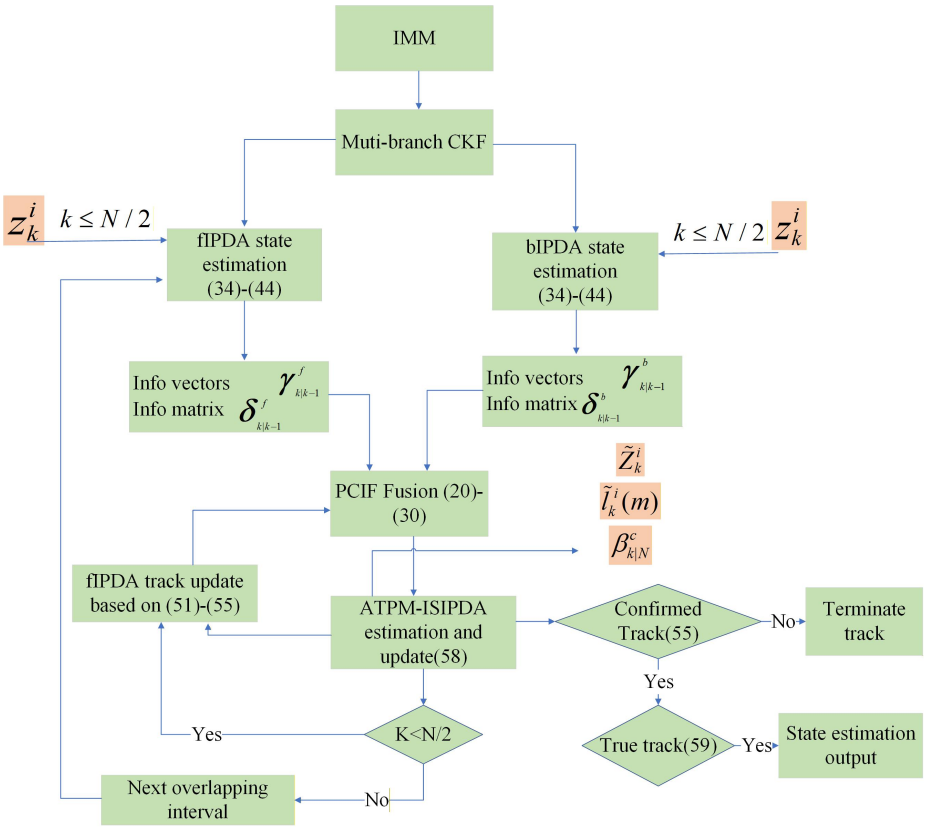

Fig. 2. Improved fixed lag smoothing data association algorithm.

3.3 ATPM-ISIPDA Algorithm

In this section, the ATPM and PCIF have been integrated to form the complete ATPM-ISIPDA algorithm. Its performance will be evaluated through comparative simulations in the following section. The ATPM-ISIPDA algorithm steps are described below.

1) Initialization

In any scan k, the state estimate $\hat{\mathbf{x}}^i_{k-1|k-1}$ and covariance matrix $\hat{\mathbf{P}}^i_{k-1|k-1}$ are initialized by using the two-point difference method [26].

2) Mixing model probability

$$\boldsymbol{\mu}^{jm}_{k-1|k-1} = \frac{\boldsymbol{\pi}_{jm}\boldsymbol{\mu}^{j}_{k-1|k-1}}{\sum\limits_{j=1}^{M}\boldsymbol{\pi}_{jm}\boldsymbol{\mu}^{j}_{k-1|k-1}} \tag{31}$$

where $\boldsymbol{\pi}_{jm}$ represents the Markov transition probability from model j to model m and $\boldsymbol{\mu}^{j}_{k-1|k-1}$ is the probability of the model j at time $k-1$.

3) Mixed state estimates and covariance matrices

$$\hat{\mathbf{x}}^m_{k-1|k-1} = \sum_{j=1}^{M}\hat{\mathbf{x}}^j_{k-1|k-1}\boldsymbol{\mu}^{jm}_{k-1|k-1}. \tag{32}$$

4) Forward integrated probabilistic data association (fIPDA)

The core recursive steps of the fIPDA algorithm, including state prediction, measurement validation, data association, and update, follow the standard IPDA framework [13–15]. The target trajectory state is represented by the state estimate $\mathbf{x}_k$ and the target existence event χ_k. In each iteration, the fIPDA track projects the updated probability density function $\mathrm{P}\{\chi_{k-1}, \mathbf{x}_{k-1}|Z_{k-1}\}$ from scan $k-1$ to k, yielding the predicted state by using CKF. Current measurements Z_k are incorporated to update the trajectory state. Target existence probability transitions from $k-1$ to k by a Markov chain model.

$$[\hat{\mathbf{x}}^m_{k|k-1}, \hat{\mathbf{P}}^m_{k|k-1}] = \mathrm{CKF}\left(\hat{\mathbf{x}}^m_{k-1|k-1}, \hat{\mathbf{P}}^m_{k-1|k-1}, \mathbf{F}^m, \mathbf{Q}^m\right), \tag{34}$$

$$\mathrm{P}\{\chi_k|Z_{k-1}\} = \alpha\mathrm{P}\{\chi_{k-1}|Z_{k-1}\} \tag{35}$$

where α is the target state transition probability.

$$\hat{\mathbf{P}}^m_{k-1|k-1} = \sum_{j=1}^{M}\boldsymbol{\mu}^{jm}_{k-1|k-1}\left(\hat{\mathbf{P}}^j_{k-1|k-1} + \left[(\hat{\mathbf{x}}^j_{k-1|k-1} - \hat{\mathbf{x}}^{jm}_{k-1|k-1})(\hat{\mathbf{x}}^j_{k-1|k-1} - \hat{\mathbf{x}}^{jm}_{k-1|k-1})^{\mathrm{T}}\right]\right). \tag{33}$$

The fIPDA trajectory utilizes the tracking gate (36) to validate the predicted measurements derived from (34), and the values that pass this validation criterion are regarded as valid measurements.

$$\mathbf{Z}_k^i = \left\{ (\mathbf{z}_k^i - \hat{\mathbf{z}}_{k|k-1}^i)^{\mathrm{T}} \mathbf{S}_k^{-1} (\mathbf{z}_k^i - \hat{\mathbf{z}}_{k|k-1}^i) \le \gamma \right\} \tag{36}$$

where $\mathbf{z}_k^i$ and $\hat{\mathbf{z}}_{k|k-1}^i$ are the actual measurement and the predicted measurement, respectively. γ is the constraint of the measurement selection.

The likelihood functions corresponding to the valid measurements $\mathbf{Z}_k^i$ are computed for each model.

$$l_k^i(m) = \begin{cases} \frac{1}{\sqrt{|2\pi \mathbf{S}_k|} P_{\mathrm{g}}} \exp\left(-\frac{1}{2} \left[\mathbf{z}_k^i - \hat{\mathbf{z}}_{k|k-1}^m \right]^{\mathrm{T}} (\mathbf{S}_k)^{-1} \left[\mathbf{z}_k^i - \hat{\mathbf{z}}_{k|k-1}^m \right] \right), & i > 0 \\ 0, & i = 0. \end{cases} \tag{37}$$

Every validated measurement $\mathbf{Z}_k^i$ at the current scan is associated with its corresponding target, and then the association probability $\beta_{k|k}$ is calculated.

$$\beta_{k|k}^i(m) = \frac{1}{\Lambda_k(m)} \begin{cases} 1 - P_{\mathrm{d}} P_{\mathrm{g}} & , \quad i = 0, \\ \frac{P_{\mathrm{d}} P_{\mathrm{g}} l_k^i(m)}{\rho} & , \quad i > 0 \end{cases} \tag{38}$$

where P_{d}, P_{g} and ρ are respectively the detection probability, the gating probability and the clutter density. The track likelihood ratio is computed.

$$\Lambda_k(m) = \begin{cases} 1 - P_{\mathrm{d}} P_{\mathrm{g}} + P_{\mathrm{d}} P_{\mathrm{g}} \sum\limits_i \frac{l_k^i(m)}{\rho} & , \quad i > 0 \\ 1 - P_{\mathrm{d}} P_{\mathrm{g}} & , \quad i = 0. \end{cases} \tag{39}$$

The track state $\hat{\mathbf{x}}_{k|k}^m$ and $\hat{\mathbf{P}}_{k|k}^m$ corresponding to the selected measurements in the scan for fIPDA can be derived from (40) to (43).

$$\hat{\mathbf{x}}_{k|k}^i(m) = \hat{\mathbf{x}}_{k|k-1}^m + \mathbf{K}_{k|k} \cdot \mathbf{v}_{k|k}, \tag{40}$$

$$\begin{aligned} \hat{\mathbf{P}}_{k|k}^i(m) =& \beta_k^0 \hat{\mathbf{P}}_{k|k-1}^m + \left[1 - \beta_k^0 \right] \left(\hat{\mathbf{P}}_{k|k-1}^m - \mathbf{K}_{k|k} \mathbf{S}_{k+1} \mathbf{K}_{k|k}^{\mathrm{T}} \right) \\ &+ \mathbf{K}_{k|k} \left(\sum_{i=1}^{m_k} \beta_k^i \mathbf{v}_k^i \left(\mathbf{v}_k^i \right)^{\mathrm{T}} - \mathbf{v}_k \mathbf{v}_k^{\mathrm{T}} \right), \end{aligned} \tag{41}$$

$$\mathbf{v}_{k|k} = \sum_{i=1}^{m_k} \beta_k^i \mathbf{v}_k^i, \tag{42}$$

$$\mathbf{K}_{k|k} = \frac{\mathbf{P}_{xz,k}}{\mathbf{P}_{zz,k}} \tag{43}$$

where m^k represents the count of valid measurements in the tracking gate.

The updated target existence probability for the next fIPDA iteration is calculated using the following

$$\mathrm{P}\{\chi_k | Z_k\} = \frac{\Lambda_k(m) \mathrm{P}\{\chi_k | Z_{k-1}\}}{1 - (1 - \Lambda_k(m)) \mathrm{P}\{\chi_k | Z_{k-1}\}}. \tag{44}$$

5) Backward integrated probabilistic data association (bIPDA)

The bIPDA multi-track estimates are computed by applying fIPDA derivations to the measurement sequence $Z_b = [Z_b, Z_{b+1}, \cdots, Z_N]$ in reverse chronological order. This process iterates (34)–(44), conditioning on $b+1$ and measurements Z_{b+1}. The procedures describe above provide the backward-smoothed state predictions $\hat{\mathbf{x}}_{b|b+1}^m$, $\hat{\mathbf{P}}_{b|b+1}^m$ and the probabilities of target existence $\mathrm{P}\{\chi_b | Z_{b+1}\}$. Subsequently, the bIPDA track update is executed to produce the state estimates $\hat{\mathbf{x}}_{b|b}^m$, $\hat{\mathbf{P}}_{b|b}^m$ and the probabilities of target existence $\mathrm{P}\{\chi_b | Z_k\}$ with the bIPDA framework.

6) Parallel cubature information fusion strategy for forward and backward tracks

Fusion of forward and backward tracks is achieved by integrating fIPDA and bIPDA outputs-state predictions, estimates, and target existence probabilities. If the forward and backward predictions at time k satisfy the validation criterion in (45), the resulting measurements are fused by using the PCIF to obtain the state component prediction and its corresponding covariance. Otherwise, the state component defaults to the fIPDA state prediction.

$$(\hat{\mathbf{x}}_{b|b+1}^m - \hat{\mathbf{x}}_{k|k-1}^m)^{\mathrm{T}} (\hat{\mathbf{P}}_{b|b+1}^m + \hat{\mathbf{P}}_{k|k-1}^m)^{-1} (\hat{\mathbf{x}}_{b|b+1}^m - \hat{\mathbf{x}}_{k|k-1}^m) \le \gamma \tag{45}$$

where the superscript c represents the ISIPDA component prediction in (46). This superscript denotes the component resulting from the fusion of forward and backward predictions, as defined in (46). The results of PCIF fusion can be obtained from (20)–(40).

Furthermore, the corresponding likelihood functions (47) and the likelihood ratio of the predicted smoothing track associated with backward prediction (48) are generated by verifying the track pairs of the gates.

$$l_{N\backslash k}^{i,c}(m) = \begin{cases} \mathcal{N}(\hat{\mathbf{x}}_{b|b+1}^m, \hat{\mathbf{x}}_{k|k-1}^m, \hat{\mathbf{P}}_{b|b+1}^m + \hat{\mathbf{P}}_{k|k-1}^m) / P_{\mathrm{g}}, & i > 0 \\ 0, & i = 0, \end{cases} \tag{47}$$

$$\Lambda_{N\backslash k} = 1 - P_{\mathrm{d}}^{'} P_{\mathrm{g}} + P_{\mathrm{d}}^{'} P_{\mathrm{g}} \sum_i \frac{l_{N\backslash k}^i(m)}{\rho^{'}} \tag{48}$$

where $\rho^{'} = \frac{n\mathrm{Tracks}}{V}$ is the bIPDA false track clutter density. $P_{\mathrm{d}}^{'} = 1 - (1 - P_{\mathrm{d}})^{N-k+1}$ represents the likelihood of target detection with the interval $[k, N]$ by both forward and backward tracking tracks. $N\backslash k$ represents the exclusion of the current measurement Z_k from the smoothing interval.

$$[\hat{\mathbf{x}}_k^c(m), \hat{\mathbf{P}}_k^c(m)] = \begin{cases} [\hat{\mathbf{x}}_{k|k-1}^m, \hat{\mathbf{P}}_{k|k-1}^m] & , \quad \text{if } bIPDA \text{ is not valid track} \\ PCIF(\hat{\mathbf{x}}_{b|b+1}^m, \hat{\mathbf{x}}_{k|k-1}^m, \hat{\mathbf{P}}_{b|b+1}^m + \hat{\mathbf{P}}_{k|k-1}^m) & , \quad \text{if } bIPDA \text{ is the valid track} \end{cases} \tag{46}$$

The predicted smoothing track calculates the component association probability for validated b^{th} track using (49).

$$\beta^c_{N\backslash k}(m) = \frac{\beta^c_{k|k-1}}{\Lambda_{N\backslash k}} \begin{cases} 1 - P'_{\text{d}} P_{\text{g}} & , \quad \text{not valid track} \\ P'_{\text{d}} P_{\text{g}} \frac{l^i_{N\backslash k}(m)}{\rho'} & , \quad \text{valid track.} \end{cases} \tag{49}$$

The ISIPDA algorithm updates the predicted smoothing target existence probability by incorporating the predicted bIPDA target existence probability in scan k, as shown in (50).

$$P\{\chi_k|Z_{N\backslash k}\} = \frac{\Lambda_{N\backslash k} P\{\chi_k|Z_{k-1}\} P\{\chi_b|Z_{b+1}\}}{1 - \left(1 - \Lambda_{N\backslash k}\right) P\{\chi_k|Z_{k-1}\}}. \tag{50}$$

7) ATPM-ISIPDA update

Following the measurement selection process, an iterative computation of (40) through (43), $\hat{\mathbf{x}}^c_{k|N}$, $\hat{\mathbf{P}}^c_{k|N}$ obtained, conditioned on scan $N\backslash k$. This calculation process generates smooth component likelihood functions for each motion model, based on the validated measurements $\tilde{\mathbf{Z}}^i_k$.

$$\tilde{l}^{i,c}_k(m) = \begin{cases} \frac{1}{\left|\sqrt{2\pi \tilde{\mathbf{S}}_k}\right| P_{\text{g}}} \exp\left(-\frac{1}{2}\left[\tilde{\mathbf{z}}^i_k - \hat{\mathbf{z}}_{k|k-1}\right]^{\text{T}} (\tilde{\mathbf{S}}_k)^{-1} \left[(\tilde{\mathbf{z}}^i_k - \hat{\mathbf{z}}_{k|k-1})\right]\right) & i > 0 \\ 0 & i = 0. \end{cases} \tag{51}$$

The weighted combination of the likelihood functions and existence probability of the fusion components are expressed in (52) and (53), respectively.

$$\tilde{l}^i_k(m) = \sum_c \tilde{l}^{i,c}_k(m) * \beta^c_{N\backslash k}(m), \tag{52}$$

$$\beta^c_k = \beta^c_{N\backslash k}(m) \tilde{\beta}^i_k \tag{53}$$

where $\tilde{\beta}^i_k$ can be obtained by substituting $\tilde{l}^{i,c}_k(m)$ into fIPDA association probability.

The state estimation of smoothing components are calculated through the Gaussian probability density function (PDF) framework. And the predicted smoothed existence probability obtained in (44) is updated in (55).

$$\begin{gathered} \hat{\mathbf{x}}_k = \sum_c \beta^c_k \hat{\mathbf{x}}^c_{k|N}, \\ \hat{\mathbf{P}}_{k|N} = \sum_c \beta^c_k \left(\hat{\mathbf{P}}^c_{k|N} + \hat{\mathbf{x}}^c_{k|N} \left(\hat{\mathbf{x}}^c_{k|N}\right)^{\text{T}}\right) - \hat{\mathbf{x}}_{k|N} \left(\hat{\mathbf{x}}_{k|N}\right)^{\text{T}}, \end{gathered} \tag{54}$$

$$\text{P}\{\chi_k \mid Z_N\} = \frac{\tilde{\Lambda}_{N\backslash k} \text{P}\{\chi_k \mid Z_{N\backslash k}\}}{1 - \left(1 - \tilde{\Lambda}_{N\backslash k}\right) \text{P}\{\chi_k \mid Z_{N\backslash k}\}}. \tag{55}$$

8) Model probability update and estimation of the trajectory state

The likelihood function is obtained by weighted combination of the predicted model probabilities.

$$l^i_k = \sum_{m=1}^{M} \mu_{k|k-1}(m) \tilde{l}^i_k(m). \tag{56}$$

The weighted likelihood function obtained from (56) the i^{th} scan is utilized to update the data association probability β^i_k. The current scan model probability can be derived in (57).

$$\mu_{k|k}(m) = \sum_{i \geq 0} \beta^i_k \mu^i_{k|k}(m). \tag{57}$$

At scan k, the target trajectory state estimate undergoes a conditional update process based on the i^{th} measurement and the m^{th} model, as derived from (40) and (41). The adaptive probability transition matrix is updated through (19). Finally, in (58), the predicted estimates for all models are weighted and combined to obtain the updated state estimate.

$$\begin{gathered} \hat{\mathbf{x}}_{k|k} = \sum_{m=1}^{M} \mu_{k|k}(m) \hat{\mathbf{x}}_{k|k}(m) \\ \hat{\mathbf{P}}_{k|k} = \sum_{m=1}^{M} \mu_{k|k}(m) (\hat{\mathbf{P}}_{k|k}(m) + \hat{\mathbf{x}}_{k|k}(m) \hat{\mathbf{x}}^{\text{T}}_{k|k}(m)) - \hat{\mathbf{x}}_{k|k} \hat{\mathbf{x}}^{\text{T}}_{k|k} \end{gathered} \tag{58}$$

The FTD procedure is similar to FLSIPDA, where the smoothed target existence probability is used to confirm/terminate track based on the predefined confirmation/termination threshold. A chi-squared statistical criterion is applied to the status of the confirmed track as expressed by

$$\left(\hat{\mathbf{x}}_{k|k} - \hat{\mathbf{x}}_{k-1|k-1}\right)^{\text{T}} \mathbf{P}^{-1}_{2|2} \left(\hat{\mathbf{x}}_{k|k} - \hat{\mathbf{x}}_{k-1|k-1}\right) < \eta \tag{59}$$

where $\mathbf{P}_{2|2}$ is the initialized covariance determined from the sensor measurement noise and η represents the selection threshold that depends on the false-alarm probability of the chi-squared distribution.

4. Simulation

The real maneuvering target motion trajectory with a three-dimensional space model is simulated, and the {CS, CA, CS-jerk} model set is selected to track in the simulation. The proposed ATPM-ISIPDA algorithm is implemented using MATLAB R2023b on a Windows 11 64-bit system equipped with an AMD Ryzen 7 8845H processor, 32GB RAM, and a Radeon 780M GPU, and its performance is compared with that of various tracking algorithms by 200 Monte Carlo simulations under the same simulation conditions. The results are presented in the form of the confirmed true track (CTT) rate and the root mean square error (RMSE) of position. The formula of the RMSE is given in (60).

$$RMSE_{\text{d}} = \sqrt{\frac{1}{M} \sum_{i=1}^{M} \left[\tilde{X}^2_{i,k} + \tilde{Y}^2_{i,k} + \tilde{Z}^2_{i,k}\right]} \tag{60}$$

where $\tilde{X}_{i,k}$, $\tilde{Y}_{i,k}$, $\tilde{Z}_{i,k}$ respectively represent the estimation errors between the filtered values and the ground truth in the X, Y, and Z directions and at time k during the i^{th} Monte Carlo run.

Parameter	Description	Value
P_d	detection probability	0.8
k	number of scans	140
T	time	1 s
ρ	clutter density	2×10^{-6} m^2
$\mathbf{x}$	initial position	$[5500,\ 10500,\ 10500]^T$ m
α	transition probability	0.98
γ	gate threshold	16
$\mathbf{R}$	observation noise	diag $\left[100^2 \quad 0.1^2 \quad 0.1^2\right]$

Tab. 2. Parameters for ATPM-ISIPDA.

Motion state	Motion duration	Acceleration variations in different directions
Uniform velocity level flight	1 s–20 s	—
Accelerated climb	20 s–30 s	$a_x = 0\,\mathrm{m/s^2}$, $a_y = 0\,\mathrm{m/s^2}$, $a_z = 20\,\mathrm{m/s^2}$
Turning maneuver	35 s–75 s	0.0436 rad/s
Decelerated descent	75 s–90 s	$a_x = 0\,\mathrm{m/s^2}$, $a_y = 0\,\mathrm{m/s^2}$, $a_z = -15\,\mathrm{m/s^2}$
Acceleration	90 s–100 s	$a_x = 30\,\mathrm{m/s^2}$, $a_y = -25\,\mathrm{m/s^2}$, $a_z = 0\,\mathrm{m/s^2}$
Turning maneuver	100 s–120 s	–0.0698 rad/s
Uniform velocity	120 s–140 s	—

Tab. 3. Expression of motion state.

The simulation parameters are shown in Tab. 2. All simulation parameters are set to be representative of realistic radar tracking scenarios, ensuring the validity of the obtained results. The detection probability $P_d = 0.8$ is selected to simulate real-world cluttered environments. The sampling time $T = 1$ s is aligned with the data rates typical of air traffic surveillance radars. The clutter density $\rho = 2 \times 10^{-6}$ m^2 is set to simulate a moderate-intensity clutter environment, thus presenting a stringent challenge for data association. The target existence transition probability $\alpha = 0.98$ is set to favor track continuity to prevent premature termination in clutter, while still allowing for true target disappearance. Given a Chi-square distribution for 3-dimensional measurements, a threshold of $\gamma = 16$ yields a high gate probability of $P_g \approx 0.9989$. This setting thereby ensures the effective inclusion of true measurements within the validation region. The measurement noise covariance $\mathbf{R} = \mathrm{diag}\left[100^2 \quad 0.1^2 \quad 0.1^2\right]$ reflects the accuracy of modern surveillance radars, while the process noise intensity $q = 0.1$ is calibrated to characterize the maneuver dynamics of typical aerial targets.

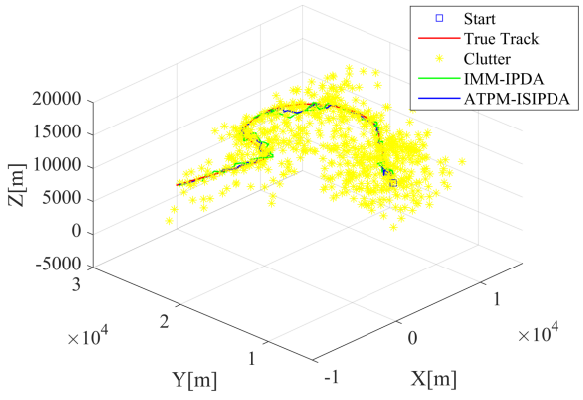

Fig. 3. Trajectory of maneuvering target in cluttered environment.

The simulated target exhibits various motion models, including constant velocity, acceleration, and turning maneuvers, demonstrating its high maneuverability, as shown in Fig. 3. The specific acceleration changes in each direction are detailed in Tab. 3.

4.1 Comparison of Smoothing Probabilistic Data Association Algorithms

The ATPM-ISIPDA algorithm is compared with IMM-IPDA, FLSIPDA, and ATPM-FLSIPDA. The IMM framework is initialized with uniform model probability $\mu = [1/3, 1/3, 1/3]$ and transition matrix $\boldsymbol{\pi} = [0.8, 0.1, 0.1; 0.1, 0.8, 0.1; 0.1, 0.1, 0.8]$, reflecting no prior maneuver knowledge and dominant steady motion. The smoothing interval length of all methods is $N = 8$, optimized in Sec. 4.4 to balance performance and computational load. The superior tracking accuracy of the proposed algorithm is quantified in Tab. 4, where it achieves the lowest RMSE in both position and velocity. These results are corroborated by Figs. 4, 5 and 6.

As shown in Fig. 4, the proposed ATPM-ISIPDA algorithm can achieve earlier track confirmation with a confirmation rate close to 100%. ATPM-ISIPDA updates the state estimation of the forward track based on the data association probability derived from the fusion of forward-backward state estimation and repeats this process until the track is terminated. However, ATPM-FLSIPDA fails to fully utilize temporal correlations in the measurement sequence, leading to imbalanced fusion of forward and backward predictions, which gradually reduces the target existence probability. The non-smoothing algorithm IMM-IPDA, relying solely on current scanning measurements for track estimation, and the time to confirm the true trajectory is much later. The traditional smooth algorithm FLSIPDA uses a single model, and it is difficult to select the correspond model during target maneuvers, resulting in potential target loss and even filter divergence.

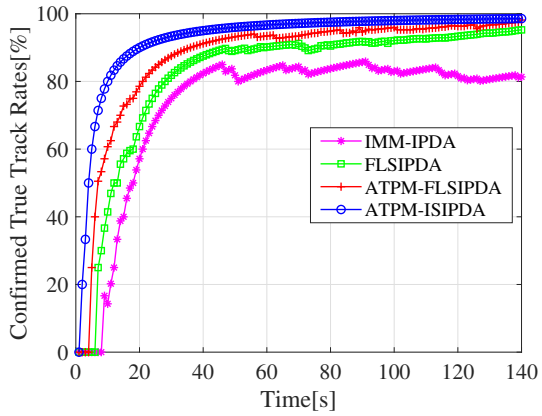

Fig. 4. CTTR of smoothing algorithms.

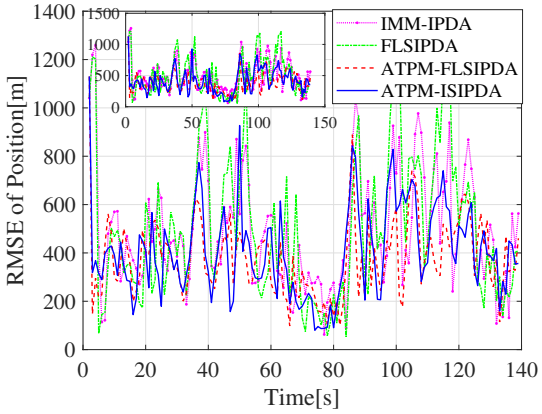

Fig. 5. The RMSE of position of smoothing algorithms.

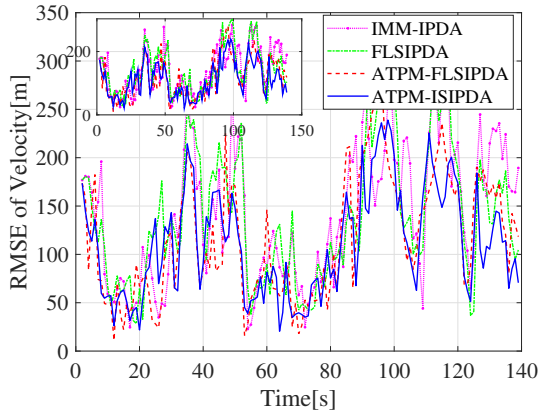

Fig. 6. The RMSE of velocity of smoothing algorithms.

Algorithm	**RMSE of position** [m]	**RMSE of velocity** [m]
IMM-IPDA	595.6464	142.8704
FLSIPDA	505.9840	139.6501
IMM-ISIPDA	485.8537	118.0662
ATPM-ISIPDA	410.3724	111.4198

Tab. 4. The average RMSE comparison of smoothing and data association algorithms.

As shown in Figs. 5, 6 and Tab. 4, the proposed algorithm significantly reduces both position RMSE and velocity RMSE overall. Compared with IMM-IPDA, FLSIPDA, and ATPM-FLSIPDA algorithms, the average position RMSE decreases by 31.1%, 18.9%, and 15.5%, respectively, and the average RMSE of velocity decreases by 22%, 20%, and 5.9%, respectively. In terms of computational cost, a single simulation trial takes 6.46 s, representing a 23.6% increase over IMM-IPDA (4.93 s) but a 9.5% decrease relative to FLSIPDA (7.14 s), while being comparable to ATPM-FLSIPDA (6.5 s). This demonstrates that the substantial gains in tracking accuracy are achieved at a modest and well-justified computational expense. During target maneuvers, the adaptive transition probability matrix will be quickly adjusted to match the current motion model. Furthermore, the parallel cubature information filter can effectively suppress nonlinear propagation errors, thereby enhancing estimation accuracy. Consequently, the proposed algorithm exhibits reduced RMSE fluctuation amplitude and superior stability. In contrast, the IMM-IPDA algorithm shows limited adaptability to abrupt motion model transitions during target maneuvers, resulting in abrupt error jumps. And it relies on current-time measurements for state prediction, underutilizing historical sensor data, which leads to the incase of the position RMSE. Although the FLSIPDA algorithm uses future prediction to update the current estimation to improve the accuracy of state estimation, it relies on the fixed transition probability matrix and IF filter. During forward-backward fusion in nonlinear scenario, the covariance will continue to increase, leading to the decline of estimation accuracy. The ATPM-FLSIPDA algorithm improves model-switching adaptability through ATPM, but its state fusion depends solely on IF, and estimation errors will still accumulate over time.

4.2 Comparison of Adaptive Transition Probability algorithms

To evaluate the tracking performance of the proposed adaptive model transition probability algorithm, the proposed algorithm is compared with the fixed transition probability algorithm (IMM-IPDA) and the fixed transition probability improved smoothing algorithm (IMM-ISIPDA). The simulation initial conditions are set as follows: the initial model probabilities $\mu = [1/3, 1/3, 1/3]$ and the Markov transition probability matrix $\boldsymbol{\pi} = [0.8, 0.1, 0.1; 0.1, 0.8, 0.1; 0.1, 0.1, 0.8]$. The results are shown in Figs. 7–11 and Tab. 5.

As shown in Figs. 7, 8 and 9, the fixed transition probability algorithm can achieve the corresponding model matching at each moving stage of the target, but there are problems with low matching accuracy and delayed model probability updates during maneuver transitions. The proposed algorithm improves the model matching probability, making model transitions more accurate and better correspond with the true motion dynamics of the target.

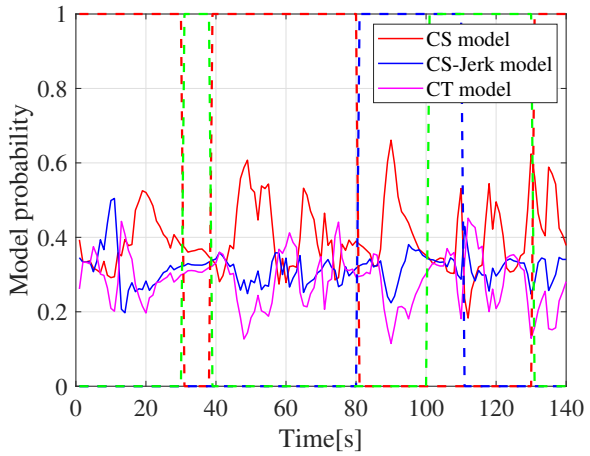

Fig. 7. Model probability for IMM-IPDA.

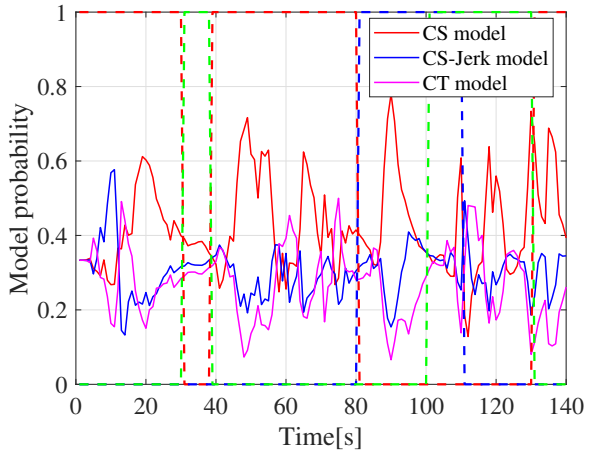

Fig. 8. Model probability for IMM- FLSIPDA.

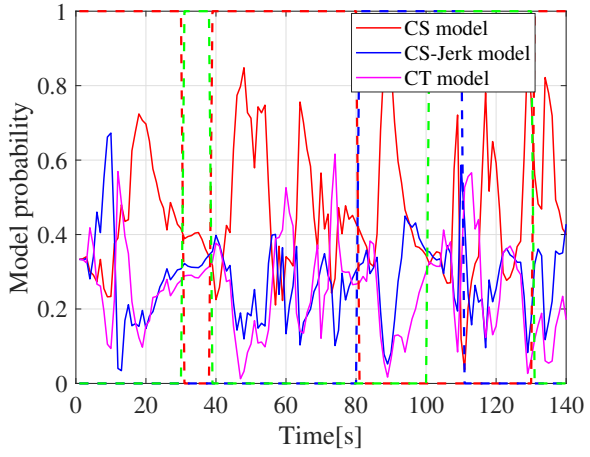

Fig. 9. Model probability for ATPM-ISIPDA.

Algorithm	**RMSE of Position** [m]	**RMSE of Velocity** [m]
IMM-IPDA	659.2814	159.5977
IMM-ISIPDA	623.5868	138.5563
ATPM-ISIPDA	511.0745	121.2613

Tab. 5. The average RMSE comparison of algorithms with fixed vs adaptive transition probability.

To assess the contribution of the adaptive transition probability matrix, Table 5 presents a focused comparison of algorithms differing primarily in the use of fixed and adaptive model switching. The results confirm that the proposed algorithm mitigates estimation errors across various maneuvering scenarios, as shown in Figs. 10, 11 and Tab. 5. The average position RMSE of the proposed algorithm decreased by 6.51%, 5.17%, 7.14% respectively, and the average RMSE of velocity decreased by 10.60%, 8.12%, and 7.51% respectively. During periods without state changes, the adaptive IMM algorithm shows limited improvement over the standard IMM algorithm, as the target motion pattern remains relatively unchanged. However, due to target state changes at 20 s, 30 s, 35 s, 75 s, 85 s, and 120 s, the adaptive transition probability matrix will quickly adjust to match the current motion model. Therefore, the ATPM-ISIPDA algorithm will have significant lower position RMSE and velocity RMSE compared to the methods in IMM-ISIPDA and IMM-IPDA.

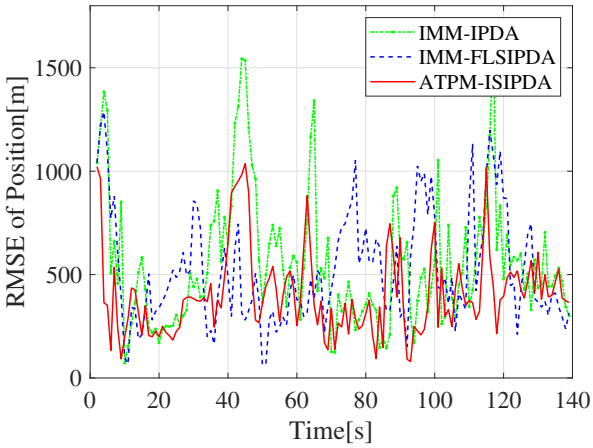

Fig. 10. The RMSE of Position for different algorithms.

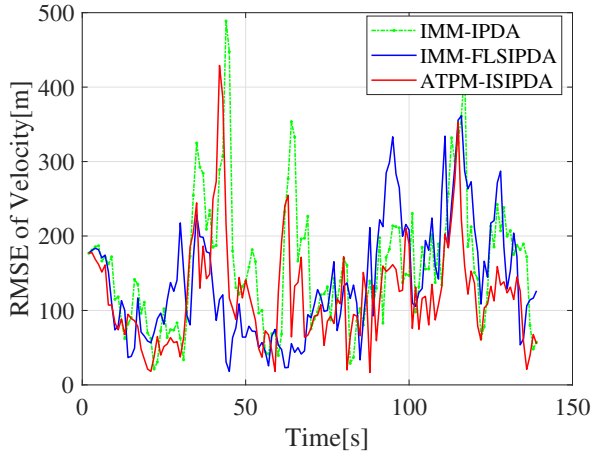

Fig. 11. The RMSE of Velocity for different algorithms.

4.3 Comparison Under Different Clutter Densities

Due to the significant impact of clutter on target tracking performance, simulation tests are conducted to evaluate the improved algorithm in different clutter density environments. The clutter densities are set to low, medium, and high levels, corresponding to $\rho_1 = 1 \times 10^{-6}\,\mathrm{m}^2$, $\rho_2 = 2 \times 10^{-6}\,\mathrm{m}^2$ and $\rho_3 = 4 \times 10^{-6}\,\mathrm{m}^2$, respectively, while keeping all other conditions identical. The results are shown in Figs. 12, 13, 14.

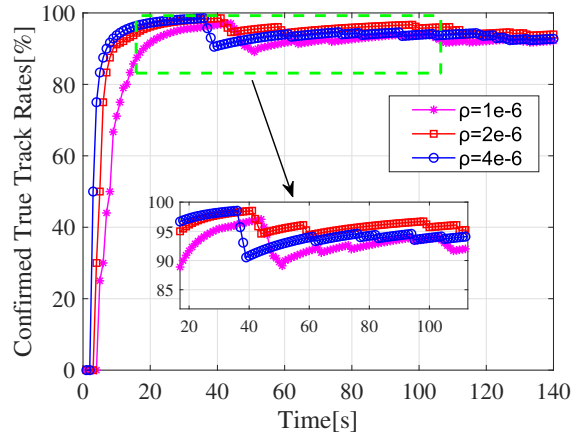

Fig. 12. CTTR of clutter density.

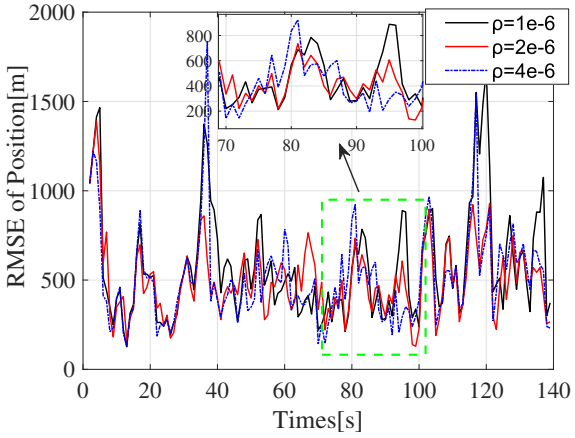

Fig. 13. The RMSE of position of clutter density.

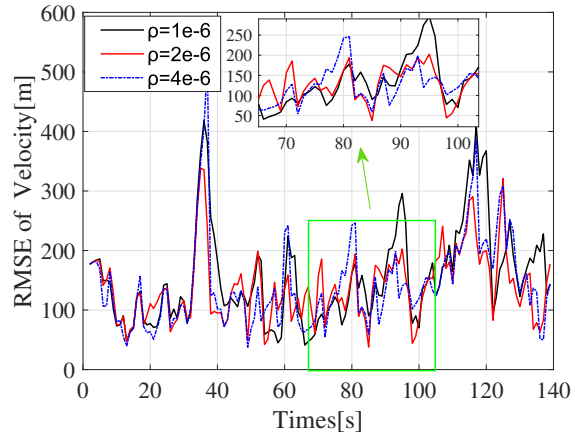

Fig. 14. The RMSE of velocity of clutter density.

As shown in the figure, the tracking algorithm adopts CKF, which enables it to adapt to the movement of the target to some extent. In lower clutter density environment, there are fewer measurements inside the tracking gate, which allows for more effective detection of target measurements. Consequently, the algorithm can achieve earlier track confirmation in low clutter density. However, during target maneuvers, the true track confirmation rate will suddenly decrease, and the position RMSE will increase. Because in high clutter density environments, the number of measurements within the tracking gate will increase, leading to a mixture of clutter and target measurements, which will have more false tracks and a higher likelihood of target loss. Thus, as the error increases, the true track confirmation rate will decrease. When the clutter density is $\rho_2 = 2 \times 10^{-6}\,\mathrm{m}^2$, the overall filtering error is reduced and CTTR is higher. This indicates that the ATPM-ISIPDA algorithm exhibits superior tracking accuracy and enhances FTD capability in environments with higher clutter density.

4.4 Comparison of Different Smoothing Interval Lengths

To further analyze the performance of the ATPM-ISIPDA algorithm, different smoothing interval lengths are investigated by selecting $N = 4, 6, 8$, and 12. The results are shown in Figs. 15, 16 and 17.

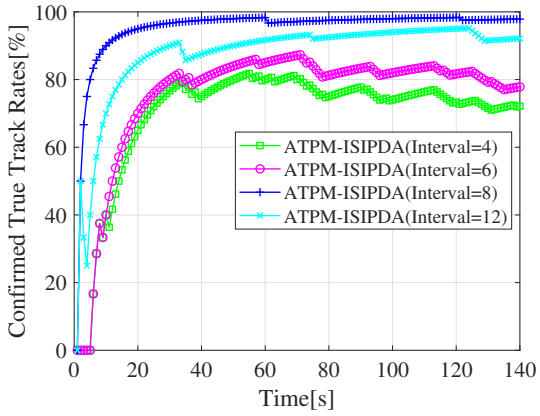

Fig. 15. CTTR of smoothing interval.

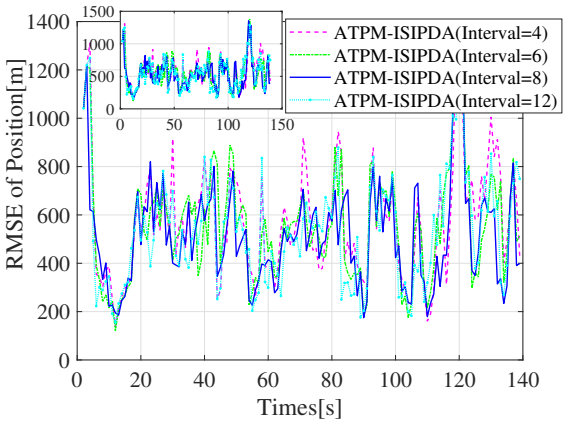

Fig. 16. The RMSE of position of smoothing interval.

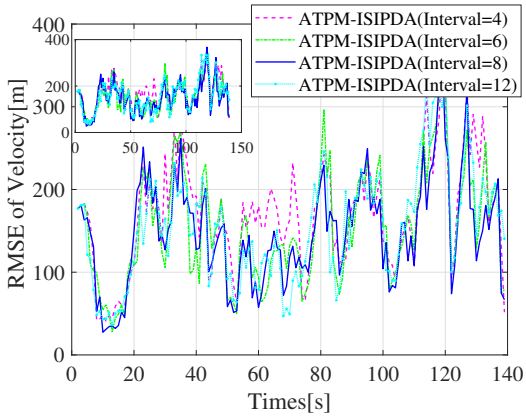

Fig. 17. The RMSE of velocity of smoothing interval.

It can be observed that the improved algorithm exhibits differences in position RMSE across the entire scanning interval. Longer intervals incorporate more future measurements, thereby reducing position RMSE compared to shorter intervals. However, they also lead to additional clutter measurements and increase susceptibility to motion model mismatch, consequently lowering the CTTR and increasing computational burden. In contrast, shorter intervals lack sufficient future measurement information, resulting in higher RMSE and delayed track confirmation. Among the evaluated configurations, $N = 8$ achieves the optimal balance between performance and computational cost. It provides significantly improved RMSE relative to $N = 4$ and $N = 6$, while avoiding the CTTR degradation and excessive computational load associated with $N = 12$.

A notable performance difference is observed at $t = 5$ s, where $N = 8$ attains 90% CTTR, while $N = 4$ and $N = 6$ remain at 0%. This performance advantage stems from two key factors: 1) the dynamic adaptation mechanism of $N = 8$ effectively integrates all available measurements ($k = 0$–$k = 5$) to obtain reliable target existence probability, and 2) the ATPM facilitates the rapid transfer of probability mass to the matched model. By contrast, shorter intervals exhibit incomplete backward-looking observation windows and only fragmented likelihood information. This results in unstable model probability estimation and delayed convergence of the track existence probability to the confirmation threshold of 0.9. Furthermore, the PCIF with $N = 8$ demonstrates enhanced capability in suppressing false associations, thereby accelerating track confirmation. These results confirm that selecting an appropriate interval based on practical scenarios is key to balancing computational efficiency and tracking performance. Ultimately, this optimization enhances both state estimation accuracy and track confirmation speed for maneuvering target tracking in cluttered environments.

4.5 Analysis and Discussion

This section provides an in-depth discussion of the above simulation results and correlates the performance of the proposed algorithm with advanced methods reported to elucidate its inherent advantages.

The model transition probability in Figs. 7, 8 and 9. reveal that the proposed algorithm facilitates rapid model switching in response to target maneuvers at 20 and 75 s. In contrast, the algorithms using fixed transition matrix, such as IMM-IPDA and IMM-ISIPDA in Figs. 7 and 8, exhibit a pronounced switching lag. This lag is a recognized manifestation of the "model competition" problem inherent to fixed-matrix IMM algorithms during maneuvers. The ATPM algorithm addresses this issue by adaptively adjusting the transition probability based on posterior information. This enhanced model responsiveness directly accounts for the superior tracking accuracy of the algorithm, as shown by the lower RMSE values in Tabs. 4 and 5.

The additional 15.5% position RMSE improvement of ATPM-ISIPDA originates from its PCIF. In contrast to the traditional IF [21] prone to linearization errors, the PCIF uses spherical-radial cubature rulesto attain third-order nonlinear estimation accuracy. This suppression of error propagation yields more balanced and stable state fusion, as demonstrated by the algorithm's smoother trajectories and lower RMSE during maneuvers in Figs. 5 and 6.

In summary, the simulation comparisons with traditional algorithms show that the ATPM-ISIPDA algorithm achieves significant performance gains by tackling two challenges: "fixed model transition probability" and "nonlinear fusion errors." The 31.1% reduction in position RMSE and 20% improvement in FTD accuracy underscore its effectiveness in handling complex maneuvers.

5. Conclusions

In conclusion, an ATPM-ISIPDA algorithm is proposed that integrates an adaptive transition probability matrix with parallel cubature information filtering in the IMM-FLSIPDA smoothing framework to enhance maneuvering target tracking performance in cluttered environments. It effectively addresses key limitations of existing tracking methods and verifies its advantages through comprehensive simulations and comparisons with representative algorithms.

The ATPM-ISIPDA overcomes the model-switching lag of traditional fixed-matrix IMM algorithms such as IMM-IPDA [17], variational Bayesian IMM [7]. These traditional algorithms use Markov transition matrix that fails to adapt to real-time target motion. In contrast, the proposed algorithm dynamically adjusts transition probability using real-time posterior model information. As verified in Sec. 4.2 and Sec. 4.5, the proposed algorithm reduces the position RMSE by 31.1% compared to IMM-IPDA and alleviates the delay in model probability updates during target coordinated turns.

The ATPM-ISIPDA resolves the suboptimal nonlinear fusion issue of linearization-based smoothing algorithms such as FLSIPDA [18] and forward-backward fusion [19]. These smoothing algorithms rely on IF, leading to accumulated errors in nonlinear radar measurement systems. The PCIF leverages spherical-radial cubature rules to achieve

third-order accuracy in nonlinear state estimation in Sec. 3.2, which suppresses error propagation more effectively than linear IF. Section 4.1 demonstrates a conclusive performance gain over FLSIPDA, with an 18.9% lower position RMSE and 13% higher FTD accuracy.

Comprehensive simulations in Secs. 4.1–4.4 further confirm the algorithm's robustness and practicality. 1) It maintains a CTTR exceeding 85% under high clutter density, demonstrating superior performance over algorithms whose efficacy degrades with sensor occlusion. 2) It exhibits stable performance across various target motion states, with smaller fluctuations in position and velocity RMSE compared to contrast algorithms.

In summary, the ATPM-ISIPDA algorithm provides a robust and efficient tracking solution, achieving a 31.1% reduction in position RMSE and a 15%–20% improvement in FTD accuracy. Its compatibility with single-radar systems makes it particularly suitable for resource-constrained environments and highly dynamic tracking scenarios. Building on it, future work will focus on extending the algorithm to multi-target scenarios and optimizing its computational efficiency for real-time applications.

References

[1] ZHANG, J., ZENG, C., TAO, H., et al. A broken-track association method for robust multi-target tracking adopting multi-view Doppler measurement information. *Signal Processing*, 2025, vol. 230, p. 1–13. DOI: 10.1016/j.sigpro.2024.109815

[2] SHAH, G. A., KHAN, S., MEMON, S. A., et al. Improvement in the tracking performance of a maneuvering target in the presence of clutter. *Sensors*, 2022, vol. 22, no. 20, p. 1–18. DOI: 10.3390/s22207848

[3] ZHONG, W. Improved IMM algorithm based on deep learning for maneuvering target tracking. In *International Russian Smart Industry Conference (SmartIndustryCon)*. Sochi (Russia), 2025, p. 878–882. DOI: 10.1109/SmartIndustryCon65166.2025.10986258

[4] NIE, C., JU, Z., SUN, Z., et al. 3D object detection and tracking based on lidar-camera fusion and IMM-UKF algorithm towards highway driving. *IEEE Transactions on Emerging Topics in Computational Intelligence*, 2023, vol. 7, no. 4, p. 1242–1252. DOI: 10.1109/TETCI.2023.3259441

[5] LUO, Y., LI, Z., LIAO, Y., et al. Adaptive Markov IMM based multiple fading factors strong tracking CKF for maneuvering hypersonic-target tracking. *Applied Sciences*, 2022, vol. 12, no. 20, p. 1–18. DOI: 10.3390/app122010395

[6] LEE, I. H., PARK, C. G. An improved interacting multiple model algorithm with adaptive transition probability matrix based on the situation. *International Journal of Control, Automation and Systems*, 2023, vol. 21, no. 10, p. 3299–3312. DOI: 10.1007/s12555-022-0989-4

[7] WANG, S., LI, R., MEN, C., et al. Adaptive IMM algorithm based on variational inference for multiple maneuvering extended targets tracking. *Advances in Astronautics*, 2025, vol. 8, p. 73–87. DOI: 10.1007/s42423-025-00173-7

[8] XIE, G., SUN, L., WEN, T., et al. Adaptive transition probability matrix-based parallel IMM algorithm. *IEEE Transactions on Systems, Man, and Cybernetics: Systems*, 2019, vol. 51, no. 5, p. 2980–2989. DOI: 10.1109/TSMC.2019.2922305

[9] YANG, Z., NIE, H., LIU, Y., et al. Robust tracking method for small and weak multiple targets under dynamic interference based on Q-IMM-MHT. *Sensors*, 2025, vol. 25, no. 4, p. 1–23. DOI: 10.3390/s25041058

[10] PETERSEN, M. E., BEARD, R. W. The integrated probabilistic data association filter adapted to Lie groups. *IEEE Transactions on Aerospace and Electronic Systems*, 2022, vol. 59, no. 3, p. 2266–2285. DOI: 10.1109/TAES.2022.3214803

[11] ZHAO, J., ZHAN, R., LIU, S., et al. Sequential joint state estimation and track extraction algorithm based on improved backward smoothing. *Remote Sensing*, 2023, vol. 15, no. 22, p. 1–25. DOI: 10.3390/rs15225369

[12] RADOSAVLJEVIĆ, Z., IVKOVIĆ, D., KOVAČEVIĆ, B. ITS efficiency analysis for multi-target tracking in a clutter environment. *Remote Sensing*, 2024, vol. 16, no. 8, p. 1–21. DOI: 10.3390/rs16081471

[13] MEMON, S., SONG, T. L., KIM, T. H. Smoothing data association for target trajectory estimation in cluttered environments. *Eurasip Journal on Advances in Signal Processing*, 2016, vol. 21, p. 1–13. DOI: 10.1186/s13634-016-0321-7

[14] KIM, M., MEMON, S. A., SHIN, M., et al. Dynamic based trajectory estimation and tracking in an uncertain environment. *Expert Systems with Applications*, 2021, vol. 177, p. 1–9. DOI: 10.1016/j.eswa.2021.114919

[15] MEMON, S. A., ULLAH, I. Detection and tracking of the trajectories of dynamic UAVs in restricted and cluttered environment. *Expert Systems with Applications*, 2021, vol. 183, p. 1–10. DOI: 10.1016/j.eswa.2021.115309

[16] KIM, H. J., XIE, Y., YANG, H., et al. An efficient indoor target tracking algorithm using TDOA measurements with applications to ultra-wideband systems. *IEEE Access*, 2019, vol. 7, p. 91435–91445. DOI: 10.1109/ACCESS.2019.2927005

[17] PARK, S. H., SONG, T. L., OH, R., et al. A new IMM interacting approach for unequal dimension states for multitarget tracking in cluttered environments. In *International Conference on Control, Automation and Information Sciences (ICCAIS)*. Xi'an (China), 2021, p. 28–33. DOI: 10.1109/ICCAIS52680.2021.9624630

[18] ZEB, N., HAMEED, G., MANZOOR, S., et al. A fixed-lag smoothing interactive multiple model tracking and interception system for maneuvering target. *Iranian Journal of Science and Technology, Transactions of Electrical Engineering*, 2020, vol. 44, no. 2, p. 605–615. DOI: 10.1007/s40998-019-00259-7

[19] MEMON, S., SON, H., MEMON, K. H., et al. Multi-scan smoothing for tracking maneuvering target trajectory in heavy cluttered environment. *IET Radar, Sonar & Navigation*, 2017, vol. 11, no. 12, p. 1815–1821. DOI: 10.1049/iet-rsn.2017.0019

[20] DONG, X., CHISCI, L., CAI, Y. An adaptive filter for nonlinear multi-sensor systems with heavy-tailed noise. *Sensors*, 2020, vol. 20, no. 23, p. 1–24. DOI: 10.3390/s20236757

[21] YANG, X., ZHANG, W. A., YU, L. A bank of decentralized extended information filters for target tracking in event-triggered WSNs. *IEEE Transactions on Systems, Man, and Cybernetics: Systems*, 2019, vol. 50, no. 9, p. 3281–3289. DOI: 10.1109/TSMC.2018.2883706

[22] DONG, P., JING, Z., LEUNG, H., et al. Variational Bayesian adaptive cubature information filter based on Wishart distribution. *IEEE Transactions on Automatic Control*, 2017, vol. 62, no. 11, p. 6051–6057. DOI: 10.1109/TAC.2017.2704442

[23] XU, W., XIAO, J., XU, D., et al. An adaptive IMM algorithm for a PD radar with improved maneuvering target tracking performance. *Remote Sensing*, 2024, vol. 16, no. 6, p. 1–23. DOI: 10.3390/rs16061051

[24] LU, C., FENG, W., LI, W., et al. An adaptive IMM filter for jump Markov systems with inaccurate noise covariances in the presence of missing measurements. *Digital Signal Processing*, 2022, vol. 127, p. 1–17. DOI: 10.1016/j.dsp.2022.103529

[25] HADAGH, M., KHALOOZADEH, H. Modified switched IMM estimator based on autoregressive extended Viterbi method for maneuvering target tracking. *Journal of Systems Engineering and Electronics*, 2018, vol. 29, no. 6, p. 1142–1157. DOI: 10.21629/JSEE.2018.06.04

[26] DE SOUZA, M. L., GUIMARÃES, A. G., PINTO, E. L. A novel algorithm for tracking a maneuvering target in clutter. *Digital Signal Processing*, 2022, vol. 126, p. 1–10. DOI: 10.1016/j.dsp.2022.103481

About the Authors ...

Yi CHENG was born in Heilongjiang Province, China, on December, 1979. She received the B.S. degree in Electrical Engineering and Automation from Harbin Institute of Technology, Heilongjiang, China, in 2001. And the M.S. degree and the Ph.D. degree in Navigation, Guidance and Control Specialty from Harbin Engineering University, Heilongjiang, China, in 2004 and 2008, respectively. She is currently an Associate Professor at Tiangong University, and engaged in radar signal processing research.

Xinyu ZHANG (corresponding author) was born in Henan Province, China. She received the B.S. degree in Electrical Engineering and Automation from Henan Normal University, Henan, China. She is a master's student majoring in Control Science and Engineering at Tiangong University; her research direction is radar target tracking and signal processing.

Yingying YAN received the B.S. degree in Electrical Engineering and Automation from Shenyang Jianzhu University, Liaoning, China. She is a master's student majoring in Control Engineering at Tiangong University; her research direction is radar track and data management.